






Detection of “diffuse” coronal He I 1083 during the April 8 2024 Solar Eclipse: evidence for terrestrial atmospheric scattering origin

Momchil E. Molnar^{1,2}  · Roberto Casini¹  ·
Paul Bryans¹  · Ben Berkey¹  ·
Kalista Tyson¹ 

© The author(s) ●●●●

Abstract

Strong He I 1083 nm atomic line signals have been previously measured during total solar eclipses at coronal heights above the lunar limb. This rather unexpected measurement has kindled a discussion about the hypothesized presence of significant amounts of neutral helium at coronal conditions. We performed spectroscopic observations of the He I 1083 nm spectroscopic region with the newly built CHEESE instrument during the April 8th 2024 total solar eclipse to test the presence of He I 1083 in the solar corona. We detected the He I 1083, the forbidden coronal line Fe XIII 1074.7 nm, as well as the chromospheric H I 1093.8 nm Paschen- γ line in our eclipse observations. The chromospheric He I 1083 and H I 1093.8 nm Paschen- γ lines are detected in the corona as well as on the lunar disc. Our findings point toward a non-solar origin of the He I 1083 signal during the April 8th 2024 eclipse that challenge the notion of abundant neutral helium in the solar corona inferred from eclipse observations.

Keywords: Corona, Structures; Eclipse Observations; Spectral Line, Intensity and Diagnostics

M. Molnar
momchil.molnar@swri.org
R. Casini
casini@ucar.edu
P. Bryans
pbryans@ucar.edu
B. Berkey
berkey@ucar.edu
K. Tyson
kalistatyson@gmail.com

¹ High Altitude Observatory, National Center for Atmospheric Research, Boulder, CO, USA

² Southwest Research Institute, Boulder, CO, USA

1. Introduction

Previous eclipse and coronagraphic observations have shown the presence of He I 1083.0 nm (He I 1083) atomic line emission in the solar corona, far away from any notable prominence contribution (Kuhn et al. 1996). In particular, the eclipse observations from Kuhn et al. (1996) show an omnipresent He I 1083 signal up to a few solar radii above the limb, with the line width corresponding to coronal temperatures, as was confirmed in following eclipse expeditions (Dima et al. 2016). This is a rather surprising finding, given that most of the helium should be fully ionized under coronal conditions (Del Zanna et al. 2020). However, coronagraphic observations with the Solar-C telescope at the Haleakala High Altitude Observatory, Hawaii (Kuhn et al. 2007; Moise et al. 2010) detected He I 1083 signal during Solar maximum in isolated coronal regions. The ubiquitous He I 1083 emission during total solar eclipses was also recently confirmed by the observations of Judge et al. (2019) during the Great American Solar eclipse of August 21 2017. The origin of the He I has been widely debated in the literature, given that the presence of a significant amount of neutral helium in the millions degree corona is physically puzzling, as well as that the very limited observations from the ground suffer from systematic uncertainties (Moise et al. 2010).

More recently, the METIS coronagraph (Antonucci et al. 2020) on Solar Orbiter (Müller et al. 2020) observed prominence eruption material at distances farther than $5 R_{\odot}$, potentially originating from the He I D₃ 587.6 nm line (Heinzel et al. 2023). The He I D₃ 587.6 nm atomic line is a subordinate line with its lower energy state being the same one as the upper one of the He I 1083 (Centeno et al. 2008). From the modeling perspective, recent numerical work by Del Zanna et al. (2020) presents a compelling evidence for bright He I 1083 signals in the lower corona similar in brightness to the regularly observed Fe XIII 1074/1079 nm line pair. This work showed how calculations including dielectronic recombination allow for a significant population of neutral helium in the lower corona, but does not explain the extensive (up to a few solar radii) He I 1083 emission observed in Kuhn et al. (1996). All this evidence for coronal He I 1083 presents an intriguing puzzle of what physical mechanism creates such an emission, and in particular if this phenomenon is of solar origin.

Detecting coronal He I 1083 is an exciting prospect for coronal magnetometry, based on the sensitivity of the He I 1083 to the coronal magnetic field through the Hanle effect (Raouafi et al. 2016). Most of the previous coronal Hanle magnetometry work has been on the Hanle effect in the Ultraviolet (UV) part of the spectrum (Raouafi et al. 1999, 2002), where many permitted atomic lines, Hanle sensitive to the coronal field, are readily observed (Khan & Nagaraju 2022; Khan et al. 2024). However, UV polarimetry is extremely challenging and currently unavailable for routine solar observations (Casini et al. 2023; Caspi et al. 2023). The advantage of using He I 1083 for the purpose of Hanle-based coronal magnetometry is the combination of its brightness and location in the infrared (IR) part of the spectrum, making it readily observable with current instrumentation (Molnar & Casini 2024). Furthermore, the He I 1083 magnetic field sensitivity regime is very similar to the measured magnetic field strengths in the solar corona (Yang et al. 2020).

However, there is the well established observational finding that strong chromospheric lines (such as the Ca II H/K and the H I Balmer series lines) are observed in the solar corona during total solar eclipses in the blue part of the visible spectrum (e.g. Grotrian 1934; Colacevic 1952; Migeotte & Rosen 1955; Deutsch & Righini 1964). This puzzling finding dates back to the beginning of the 20th century and invited two opposing physical explanations: cool, “diffuse”, prominence material dispersed in the million degree corona (Bappu et al. 1972); or, a scattering origin of the signal in the local environment around Earth (Caccin et al. 1971; Bappu et al. 1972). An eclipse experiment by Stellmacher & Koutchmy (1974) showed strong evidence for the non-coronal origin of the observed chromospheric lines in the blue part of the spectrum, by detecting them contemporaneously on the lunar disc and in the solar corona. Stellmacher & Koutchmy (1974) demonstrated that the cool chromospheric lines in the blue part of the spectrum, seen on the lunar disc, have line width dependence on their rest wavelength following a relation expected if they originated from Rayleigh scattering in the terrestrial atmosphere. The recent observations by Judge et al. (2019) also show a brightening of the He I 1083 emission closer to second and third contacts, which agrees with the terrestrial atmospheric scattering origin hypothesis.

The unsettled state of knowledge about the origin of the “diffuse” coronal He I 1083 outlined in the previous paragraphs motivated us to perform eclipse measurements of the near-IR coronal spectrum during the April 8 2024 eclipse with the required spectral resolution and field-of-view to test the terrestrial atmospheric scattering origin hypothesis. In particular, following the approach from Stellmacher & Koutchmy (1974) we planned to observe the lunar disc as well as the corona during the total solar eclipse on April 8 2024. We built the Coronal Helium Emission Spectrograph Experiment (CHEESE) designed specifically to have large field of view, to be able to observe both the lunar disc and the corona, as well as high enough spectral resolution, crucial for resolving the He I line and measuring its line width (Kuhn et al. 1996). In this paper we present the results from the NCAR/HAO April 8 2024 eclipse expedition where we deployed (CHEESE) to measure the diffuse He I 1083 coronal component. We describe the instrument design and the observational campaign in Section 2. We present our findings in Section 3 and their implications in Section 4.

2. Observations

2.1. Instrument design

CHEESE is a diffraction grating spectrograph operating in the near-IR designed to reproduce the previous observations of He I 1083 in the corona (Kuhn et al. 1996). The optical layout of the system is presented in Figure 1 panel (a). An actual photo of the assembled spectrograph is shown in Figure 1 panel (b), with some of the essential components labeled. We used a commercially available $f/4$ Newtonian Skywatcher Quattro 150P telescope with primary mirror of $D=15$ cm and focal length of 600 mm. A $40 \mu\text{m}$ slit was placed in the primary focus of the

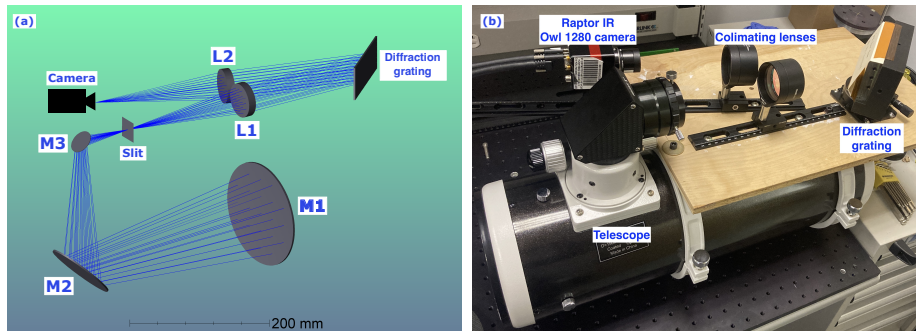


Figure 1. Overview of the CHEESE instrument. **Panel (a):** Optical layout of the CHEESE instrument produced with the Zeemax software suite. The primary and secondary mirrors of the Skywatcher Quattro telescope correspond to $M1$ and $M2$, the diagonal 90° mirror to $M3$, and the two collimating lenses in the spectrograph are labeled as $L1$ and $L2$. **Panel (b):** CHEESE during laboratory bench assembly in HAO/NCAR. The essential optical components and the camera are labeled. Note that during the actual observations the spectrograph was housed inside a thermally insulated light-tight enclosure to protect it from the ambient environment.

telescope while mounted on a helical focuser for fine position adjustments. We used a Bausch and Lomb diffraction grating, with a blaze angle of 17.5° in inverse configuration (i.e., at 72.5° blaze) with 600 lines/mm. The grating was mounted on a 3D-printed adapter to a rotational stage for fine adjustment of the beam incidence angle (and the resultant observed wavelength range). We use two near-IR ThorLabs achromatic lenses ($L1$ and $L2$ in Figure 1) with 200 mm focal length to illuminate the grating with the collimated beam and then image the dispersed spectrum on the camera. Raptor IR Owl 1280 InGaS camera was used for this experiment, suitable with its high quantum efficiency (QE 90% at $1 \mu\text{m}$), large $10 \mu\text{m}$ pixel size, and low readout and thermal noise properties. The camera has active internal cooling, which we enhanced with externally mounted radiators. This allowed for the stable operation of the camera with the detector cooled to a temperature of 1°C . Despite the ability of the camera to sustain lower temperatures, we decided against running it below freezing to avoid any condensation buildup on its entrance window.

We operated CHEESE in the second diffraction order for the best combination of efficiency and dispersion. To reject overlapping orders on the detector, an additional 980 nm high pass order sorting filter is required, which was mounted right before the camera body, to remove contribution from higher orders; on the upper end of the wavelength range, the camera QE efficiency drops to effectively zero above $1.8 \mu\text{m}$, which effectively rejects the overlapping lower order contributions. The resulting spectrograph has predicted spectral resolution of $R \sim 9,600$ and a plate scale of $3.43''/\text{pixel}$. Given an estimated vignetting of 0.9, we estimated He I 1083 signal-to-noise ratio (SNR) of a few hundred after 1 minute of integration under coronal conditions, such as the ones described in Kuhn et al. (1996). The 1 cm slit of CHEESE spans $58'$ on the plane of the sky, allowing for sampling of both the lunar disc and the corona simultaneously, as shown in Figure 2. CHEESE was mounted on a Losmandy GM-8 equatorial mount with a Gemini-1 guiding system; the telescope and spectrograph weigh

about 23 pounds, well below the limit of the guiding system and light enough for swift (re-)deployment, as proved necessary during our expedition. The 3D printed slit and diffraction grating mount designs are publicly available in the repository associated with this publication ¹.

2.2. Observational campaign

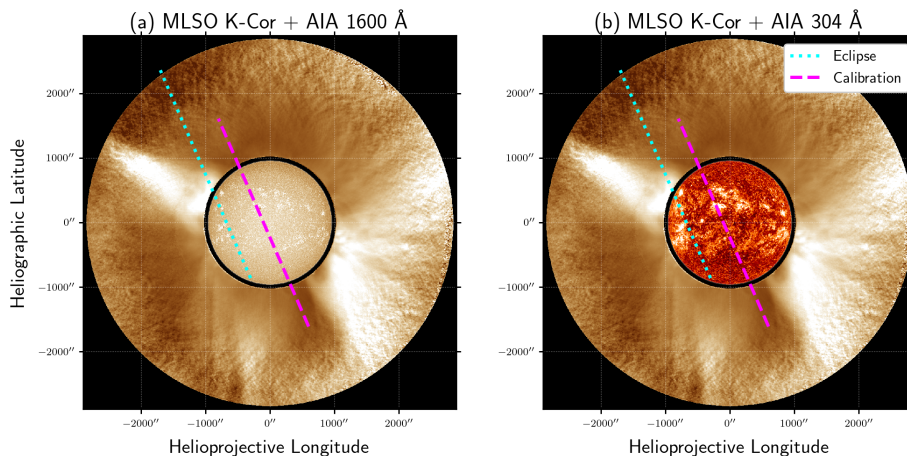


Figure 2. Composite coronal images from the MLSO/K-Cor and SDO/AIA instruments of the observed regions with CHEESE during the eclipse at 2024 April 8 13:00 UT. **Panel (a):** solar disc is from the AIA 1600 Å channel; **Panel (b):** same as panel (a) for the AIA 304 Å channel. The corona above $1.01 R_{\odot}$ is imaged by the MLSO/K-Cor white light coronagraph on April 9 2024, the day after the eclipse. The magenta dashed line corresponds to the the approximate slit location during the CHEESE calibration and the cyan dotted line shows the approximate slit location during totality.

The NCAR/HAO expedition observed the total solar eclipse from Dardanelle, Arkansas, USA at geographical coordinates N $35^{\circ}12'14.7''$ W $93^{\circ}12'16.5''$. Our original intent was to observe the eclipse from a location close to San Antonio, Texas, based on the historically favorable climatological record. However, adverse weather forecasts led us to relocate our eclipse observing campaign to Dardanelle, AR. We set our instruments on the night before the eclipse (April 7-8 2024) with clear skies allowing us to align our mounts. The weather during the eclipse was stable with thin high cloud cover present during totality.

Overview of the solar coronal conditions on the day of the eclipse is shown in Figure 2, where composite images with data from SDO/AIA (Lemen et al. 2012) from April 8 2024 and the whitelight coronagraph from the Mauna Loa Solar Observatory (MLSO) K-Cor (de Wijn et al. 2012) from April 9 2024 (the day after the eclipse) are combined. The MLSO K-Cor observes the whitelight continuum corona in the region of 780 nm and the data product which we show in Figure 2 has a normalized radial gradient filter applied. We have indicated on

¹<https://github.com/momomolnar/CHEESE-data>

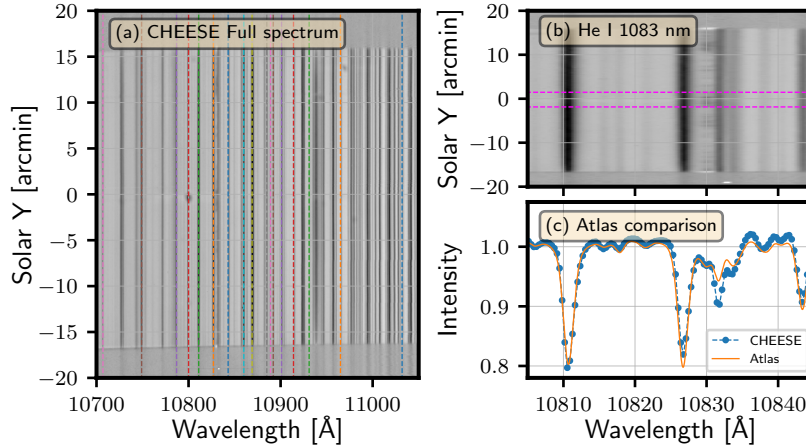


Figure 3. Calibration on-disc data taken at 13:23 UT Apr 8 2024. **Panel (a):** full CHEESE spectrum with dispersion correction applied. The absorption lines used for the dispersion and rotation corrections are marked as thin dashed lines. **Panel (b):** the region around the He I 1083, where the Si I 10827 Å and He I 1083 lines are clearly seen. The dashed magenta lines mark the region used for studying the average spectral properties (see next panel). **Panel (c):** Averaged CHEESE observation (blue dots) compared with an instrument model based on solar atlas data (dashed orange).

Figure 2 the approximate locations of the CHEESE slit during the calibration process as the dashed magenta line, and its approximate location during the eclipse observations as the dotted cyan one.

We used the sunspot group associated with NOAA AR 13628, located close to disc center, to act as a fiducial line to remove the image rotation of the spectrum on the detector, which was measured to be about 1.5° . The wavelength dispersion of the spectrograph was then determined by finding the precise location of 17 known spectral infrared lines using the atlas of Dellbouille et al. (1981), hosted online on the BASS2000 webpage². The calibration spectral lines are shown in panel (a) of Figure 3 as the thin dashed colored lines. We chose the particular calibration lines to be well separated from the surrounding (complex) spectral features and blends. We computed the dispersion of our spectrograph by fitting the centroids of the reference spectral lines and then fitting a parabolic dispersion relationship for each row of the detector. Then, for every image row the parabolic wavelength dependence was used to resample the data uniformly in wavelength. The resulting uniformly sampled spectrum is shown in panels (a) and (b) of Figure 3. The wavelength dispersion mapping we found was smooth across the detector, showing the fidelity of the recovered spectra.

In panel (b) of Figure 3 we demonstrate the presence (and detectability) of He I 1083 as well as the nearby Si I 1082.7 nm lines observed on the solar disc. In particular, note the He I 1083 line going into emission above the solar limb, noted as the brightening in it in the continuum averaged spectrum in panel

²<https://bass2000.obspm.fr/>

(b) of Figure 3. In panel (c) of Figure 3 we present a comparison between the CHEESE data and the solar atlas from Neckel (1999). The average spectrum of the data between the cyan curves in panel Figure 3 (b) is shown as the blue dots in panel (c), and the solar atlas fits are presented as the orange line. We fitted the solar atlas to a subsample of the CHEESE data in panel (b) of Figure 3 marked as the region between the magenta dashed lines. We fitted the atlas data by rescaling its intensity level, including a scattered light component (flat background), and degrading it with a spectral resolution (a Gaussian line spread function) with its width kept as a free parameter. The resulting fit gave us an estimate of the effective resolving power of the spectrograph as well as an estimate of the amount of scattered light, based on the flat (gray) component needed to be included to fit the spectrum to the atlas. Based on the fitting of the solar atlas spectrum to our measurements we estimated that CHEESE was observing with an effective spectral resolution of about $R \sim 7000$. This effective spectral resolution shows that our spectrograph behaves similarly to its designed specification; most importantly it is able to detect (and resolve) the He I 1083 line successfully.

3. Results from the eclipse observations

During the eclipse, we pointed our instrument towards the east solar limb where a bright streamer was present on the day of the eclipse, as shown in Figure 2. We chose this pointing to maximize the likelihood of detecting coronal He I signal, by observing a coronal region of enhanced plasma density.

The CHEESE data collected during the eclipse totality suffered from a dynamic range issue due to the internal data reduction performed onboard the camera. This step reduced the camera dynamic range to be effectively 12-bit compared to the detector well depth of 16 bits. Since our slit was crossing the chromosphere, bright chromospheric material ($\sim 10^5 \mu\text{B}_\odot$) in the He I 1083 drove the response of the camera such that the anticipated weak coronal signals ($\sim 10 \mu\text{B}_\odot$) were outside of the effective dynamic range of the camera. Hence, we did not detect any coronal signals until the chromosphere was completely covered by the lunar disc, close to third contact for our east-pointing slit configuration. During the time period around third contact, the Moon covered almost all of the previously visible bright chromospheric signal and our measurements started to exhibit the coronal Fe XIII 1074.7 nm line, as well as the other spectral signals described below. We co-added 125 exposures (10 seconds of effective exposure time) taken between 18:54:17-18:54:28, which is 10 seconds after third contact for the exact observing location. Since we were observing on the east limb, our slit was not crossing the flash spectrum.

The CHEESE data from the totality are shown in Figure 4. We have applied the wavelength dispersion mapping from the on-disk calibration observations taken earlier in the day, presented in Figure 3. Panel (a) of Figure 4 shows the full detector spectrum averaged over the time period between 18:54:17-18:54:28 UT. The approximate location of the lunar limb is the green dashed line, and one can clearly see the He I 1083 line, observed both above and below the limb.

However, the coronal Fe XIII 1074.7 nm line is only detected above the solar limb, in the coronal region of the data. Note that over the temporal averaging window, the lunar limb moves about 1.2 arcmin in the upward direction of Figure 4 panel (a); hence care should be taken in the interpretation of the region close to the limb. Furthermore, the H I 1093.8 nm Paschen- γ line is detected clearly on the lunar disc and not so much in the coronal region, due to the increased background and noise levels, as shown in panels (a) and (d) in the Figure 4. We note that the detection of those lines is further supported by the precise coincidence of their detected wavelength locations, as shown in panels (b)-(d) of Figure 4.

We measured the line width of the Fe XIII 1074.7 and the He I 1083.0 lines by fitting their spectral shapes after averaging over 3 pixels along the slit. We fitted the line profiles with Gaussian line shapes and a linear background to take into account the varying background continuum level. The results from the line fitting are shown in panel (e) of Figure 4, where the line width of the Fe XIII 1074 nm and the He I 1083 nm lines are shown as the orange and blue markers, as well as the He I 1083 line intensity shown in green. The standard deviation of the inferred parameters, provided from the Levenberg–Marquardt fitting routine, are presented as the error bars in the figure. We note that on average the coronal Fe XIII 1074 nm line width agrees with the previous work by Schad et al. (2023). In particular, applying Equation 14 from Schad et al. (2024) to estimate the plasma temperature responsible for the line width of the lines (assuming no thermal broadening), the Fe XIII 1074 line hints at coronal formation temperatures of $\sim 10^6$ K. However, the observed He I 1083 line width in the corona is significantly lower than the line width of the Fe XIII 1074 nm; based on the aforementioned approach used, the plasma temperature responsible for the thermal broadening of the He I 1083 in the corona is on the order of 10^5 K.

Also, one should note that the He I 1083 intensity and line width are increasing on the lunar disc toward the bottom of the slit. This directional dependence of the He I 1083 line intensity corresponds to a decreasing separation of the slit from the flash spectrum. Both of those evidence suggest terrestrial atmospheric scattering origin of the observed He I 1083 signal.

4. Conclusions

We present the first results from the CHEESE experiment during the April 8 2024 solar eclipse. We designed and built a near-IR spectrograph with sufficient resolution to observe the He I 1083 nm line, and to test the origin of the “diffuse” neutral helium corona. Testing this hypothesis drove the design requirements of CHEESE, in particular the need for sufficient spectral resolution to be able to discern the thermal width of the line and a large enough field of view to be able to observe a significant part of the lunar disc and the corona at the same time. We built a classical slit spectrograph with $R \sim 9000$ in its current setting (depending on the width of the slit used) as shown in Section 2.1.

We deployed successfully CHEESE at Dardanelle, AR during the April 8th 2024 total solar eclipse. Our calibration measurements of the solar disc showed that the instrument met its design requirements. In particular, we were able

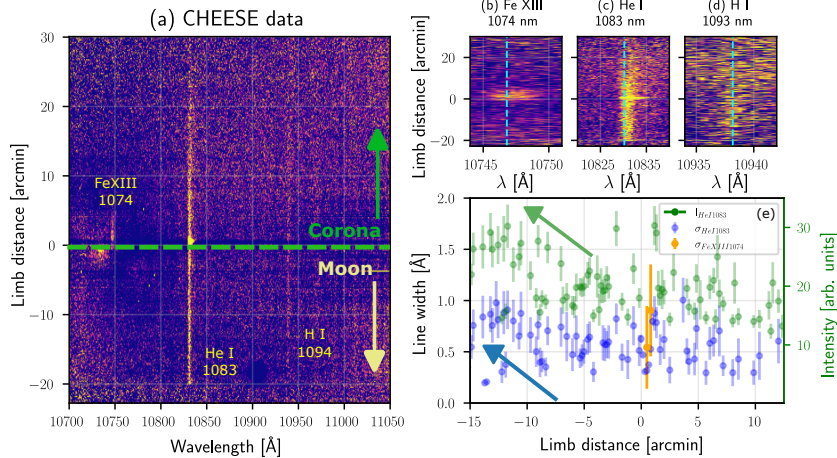


Figure 4. Results from the eclipse observations. **Panel (a):** Processed CHEESE spectrum obtained during the total solar eclipse between 11:54:17 - 11:54:28 UT on April 8th 2024. In total we had. Note the ever present He I 1083.0 nm line, as well as the Fe XIII 1074 nm line. A very dim spectral line is detected at the precise location of the chromospheric H I Paschen- γ 1093.8 nm line. **Panels (b)-(d):** Zoom in over the detected spectral lines in the CHEESE data, in order: (b) Fe XIII 1074.7 nm; (c) He I 1083.0 nm; (d) H I Paschen- γ 1093.8 nm. The cyan line marks the reference wavelength. **Panel (e):** Line width in Angstrom of the detected He I 1083 (in blue) and the Fe XIII 1074 nm line (in orange), and the He I 1083 line intensity (green).

to observe the He I 1083 on the disc right before the eclipse with sufficient spectral resolution to discern it from the nearby Si I 1082.7 nm line. Despite the technical difficulties during the eclipse, described in Section 3, CHEESE managed to collect data successfully. As shown clearly in Figure 4, we observed the coronal Fe XIII 1074.7 nm line, as well as the He I 1083 and the H I Paschen- γ 1093.8 nm lines. The coronal Fe XIII 1074.7 nm line was observed only above the lunar limb in the solar corona, whereas the strong chromospheric lines were observed both above the limb and on the lunar disc.

Similarly to the conclusions in Stellmacher & Koutchmy (1974) for the chromospheric lines in the blue part of the visible spectrum, we believe that we observed during the total solar eclipse observations a local (between us and the lunar surface) origin of the He I 1083 (and the H I Paschen- γ line) due to its presence on the lunar disc. This agrees well with the temporal variation of the He I 1083 intensity shown by Judge et al. (2019) close to second and third contacts. We do not anticipate an terrestrial exospheric origin of the signal (Lammer et al. 2022), coming from He I ions, because this cannot explain readily the presence of the previously observed lines of Ca II in the blue part of the spectrum by Stellmacher & Koutchmy (1974). However, this observation grants a further repeat of this observations and we believe measurements above (much of) the atmosphere, in conditions of significantly lower sky brightness, such as the CORSAIR balloon, would judge a definitive verdict on the scattering hypothesis we further in this work.

In conclusion, we believe that our measurements support the idea that the previous work on eclipse He I 1083 signals in the strong corona are originating from the local environment between the lunar disc and our slit. In particular, following up on the previous work by Stellmacher & Koutchmy (1974) who measured the brightness of the scattered Hydrogen Balmer series lines on the lunar disc, we believe we observe a similar phenomenon. However, since we are observing in the near infrared part of the spectrum the contribution from Mie scattering should be also noted, compared to the Rayleigh scattering case of Stellmacher & Koutchmy (1974) in the blue part of the spectrum they observed. We believe that our measurements affirm the terrestrial atmospheric origin of the “cool” helium corona.

Acknowledgments The authors express their gratitude to the members of the HAO Eclipse Expedition for their support. MEM would like to especially thank Cory Buhay, Clementine Mitchell, and Vesta Alexander-Molnar for their unconditional support with the incessantly arising challenges during the expedition. We also want to thank Skylar Shaver (CU/ LASP) for generously accommodating the HAO eclipse expedition in her home in Dardanelle, AR. The authors would like to thank Dr. Kevin Reardon (NSO) for the enriching discussions, in particular about the eclipse science results from the middle of the twentieth century. The National Center for Atmospheric Research is a major facility sponsored by the NSF under Cooperative Agreement No. 1852977. MEM was supported by the ASP Postdoctoral fellowship. This work was supported by NSF Grant Award 2504074. The K-Cor data is a courtesy of the Mauna Loa Solar Observatory, operated by the High Altitude Observatory, as part of the National Center for Atmospheric Research (NCAR). The following Python packages were used in this work: `astropy` (Astropy Collaboration et al. 2022); `numpy` (Harris et al. 2020); `scipy` (Virtanen et al. 2020); and `sunpy` (The SunPy Community et al. 2020). This research has made use of the Astrophysics Data System, funded by NASA under Cooperative Agreement 80NSSC21M00561.

References

- Antonucci, E., Romoli, M., Andretta, V., et al. 2020, *Astron. Astrophys.*, 642, A10, doi: [10.1051/0004-6361/201935338](https://doi.org/10.1051/0004-6361/201935338)
- Astropy Collaboration, Price-Whelan, A. M., Lim, P. L., et al. 2022, *Astrophys. J.*, 935, 167, doi: [10.3847/1538-4357/ac7c74](https://doi.org/10.3847/1538-4357/ac7c74)
- Bappu, M. K. V., Bhattacharyya, J. C., & Sivaraman, K. R. 1972, *Sol. Phys.*, 26, 366, doi: [10.1007/BF00165277](https://doi.org/10.1007/BF00165277)
- Caccin, B., Moschi, G., Rigutti, M., & Falciani, R. 1971, *Sol. Phys.*, 17, 89, doi: [10.1007/BF00152863](https://doi.org/10.1007/BF00152863)
- Casini, R., Gibson, S., Bak-Steslicka, U., et al. 2023, in *Bulletin of the American Astronomical Society*, Vol. 55, 047, doi: [10.3847/25c2cfef.e2c303f5](https://doi.org/10.3847/25c2cfef.e2c303f5)
- Caspi, A., Seaton, D., Casini, R., et al. 2023, in *Bulletin of the American Astronomical Society*, Vol. 55, 048, doi: [10.3847/25c2cfef.b95dd671](https://doi.org/10.3847/25c2cfef.b95dd671)
- Centeno, R., Trujillo Bueno, J., Uitenbroek, H., & Collados, M. 2008, *Astrophys. J.*, 677, 742, doi: [10.1086/528680](https://doi.org/10.1086/528680)
- Colacevic, A. 1952, *Accademia Nazionale dei Lincei, Fondazione Volta*, 186

-
- de Wijn, A. G., Burkepile, J. T., Tomczyk, S., et al. 2012, in *Ground-based and Airborne Telescopes IV*, ed. L. M. Stepp, R. Gilmozzi, & H. J. Hall, Vol. 8444, International Society for Optics and Photonics (SPIE), 84443N, doi: [10.1117/12.926511](https://doi.org/10.1117/12.926511)
- Del Zanna, G., Storey, P. J., Badnell, N. R., & Andretta, V. 2020, *Astrophys. J.*, 898, 72, doi: [10.3847/1538-4357/ab9d84](https://doi.org/10.3847/1538-4357/ab9d84)
- Dellbouille, L., Roland, G., Brault, J., & Testerman, L. 1981, *Photometric Atlas of the Solar Spectrum from 1.850 to 10.000 cm⁻¹* (Tucson, Arizona, USA)
- Deutsch, A. J., & Righini, G. 1964, *Astrophys. J.*, 140, 313, doi: [10.1086/147920](https://doi.org/10.1086/147920)
- Dima, G., Kuhn, J., & Berdyugina, S. 2016, *Frontiers in Astronomy and Space Sciences*, 3, 13, doi: [10.3389/fspas.2016.00013](https://doi.org/10.3389/fspas.2016.00013)
- Grottrian, W. 1934, *Zeitschrift fuer Astrophysik*, 8, 124
- Harris, C. R., Millman, K. J., van der Walt, S. J., et al. 2020, *Nature*, 585, 357, doi: [10.1038/s41586-020-2649-2](https://doi.org/10.1038/s41586-020-2649-2)
- Heinzel, P., Jejić, S., Štěpán, J., et al. 2023, *Astrophys. J. Lett.*, 957, L10, doi: [10.3847/2041-8213/acff62](https://doi.org/10.3847/2041-8213/acff62)
- Judge, P., Tomczyk, S., Hannigan, J., & Sewell, S. 2019, *Astrophys. J.*, 877, 10, doi: [10.3847/1538-4357/ab0e04](https://doi.org/10.3847/1538-4357/ab0e04)
- Khan, R., Gibson, S. E., Casini, R., & Nagaraju, K. 2024, *Astrophys. J.*, 971, 27, doi: [10.3847/1538-4357/ad55ed](https://doi.org/10.3847/1538-4357/ad55ed)
- Khan, R., & Nagaraju, K. 2022, *Sol. Phys.*, 297, 96, doi: [10.1007/s11207-022-02024-2](https://doi.org/10.1007/s11207-022-02024-2)
- Kuhn, J. R., Arnaud, J., Jaeggli, S., Lin, H., & Moise, E. 2007, *Astrophys. J. Lett.*, 667, L203, doi: [10.1086/522370](https://doi.org/10.1086/522370)
- Kuhn, J. R., Penn, M. J., & Mann, I. 1996, *Astrophys. J. Lett.*, 456, L67, doi: [10.1086/309864](https://doi.org/10.1086/309864)
- Lammer, H., Scherf, M., Ito, Y., et al. 2022, *Space Sci. Rev.*, 218, 15, doi: [10.1007/s11214-022-00876-5](https://doi.org/10.1007/s11214-022-00876-5)
- Lemen, J. R., Title, A. M., Akin, D. J., et al. 2012, *Sol. Phys.*, 275, 17, doi: [10.1007/s11207-011-9776-8](https://doi.org/10.1007/s11207-011-9776-8)
- Migeotte, M., & Rosen, B. 1955, *Ciel et Terre*, 71, 288
- Moise, E., Raymond, J., & Kuhn, J. R. 2010, *Astrophys. J.*, 722, 1411, doi: [10.1088/0004-637X/722/2/1411](https://doi.org/10.1088/0004-637X/722/2/1411)
- Molnar, M. E., & Casini, R. 2024, *Astrophys. J.*, 977, 97, doi: [10.3847/1538-4357/ad8de4](https://doi.org/10.3847/1538-4357/ad8de4)
- Müller, D., St. Cyr, O. C., Zouganelis, I., et al. 2020, *Astron. Astrophys.*, 642, A1, doi: [10.1051/0004-6361/202038467](https://doi.org/10.1051/0004-6361/202038467)
- Neckel, H. 1999, *Sol. Phys.*, 184, 421, doi: [10.1023/A:1017165208013](https://doi.org/10.1023/A:1017165208013)
- Raouafi, N. E., Lemaire, P., & Sahal-Bréchet, S. 1999, *Astron. Astrophys.*, 345, 999
- Raouafi, N. E., Riley, P., Gibson, S., Fineschi, S., & Solanki, S. K. 2016, *Frontiers in Astronomy and Space Sciences*, 3, 20, doi: [10.3389/fspas.2016.00020](https://doi.org/10.3389/fspas.2016.00020)
- Raouafi, N. E., Sahal-Bréchet, S., & Lemaire, P. 2002, *Astron. Astrophys.*, 396, 1019, doi: [10.1051/0004-6361:20021418](https://doi.org/10.1051/0004-6361:20021418)
- Schad, T. A., Kuhn, J. R., Fehlmann, A., et al. 2023, *Astrophys. J.*, 943, 59, doi: [10.3847/1538-4357/acabbd](https://doi.org/10.3847/1538-4357/acabbd)
- Schad, T. A., Fehlmann, A., Dima, G. I., et al. 2024, *Astrophys. J.*, 965, 40, doi: [10.3847/1538-4357/ad2995](https://doi.org/10.3847/1538-4357/ad2995)
- Stellmacher, G., & Koutchmy, S. 1974, *Astron. Astrophys.*, 35, 43
- The SunPy Community, Barnes, W. T., Bobra, M. G., et al. 2020, *Astrophys. J.*, 890, 68, doi: [10.3847/1538-4357/ab4f7a](https://doi.org/10.3847/1538-4357/ab4f7a)
- Virtanen, P., Gommers, R., Oliphant, T. E., et al. 2020, *Nature Methods*, 17, 261, doi: [10.1038/s41592-019-0686-2](https://doi.org/10.1038/s41592-019-0686-2)
- Yang, Z., Bethge, C., Tian, H., et al. 2020, *Science*, 369, 694, doi: [10.1126/science.abb4462](https://doi.org/10.1126/science.abb4462)